Citation
Li, H. and Chen, W. and Hao, H. 2020. Factors influencing impact force profile and measurement accuracy in drop weight impact tests. International Journal of Impact Engineering. 145: ARTN 103688.
http://doi.org/10.1016/j.ijimpeng.2020.103688

Factors influencing impact force profile and measurement accuracy in drop weight impact tests

Huawei Li, Wensu Chen*, Hong Hao*

Center for Infrastructural Monitoring and Protection, School of Civil and Mechanical Engineering, Curtin University, Perth, Australia

* Corresponding authors:

wensu.chen@curtin.edu.au (W. Chen), hong.hao@curtin.edu.au (H. Hao)

Abstract: Drop weight tests on RC beams have been intensively reported in literature. Load cells are commonly used to measure the impact force acting on the beam. Different researchers adopted different configurations, e.g., location of load cells in the test, which could affect the impact load measurement. In addition, the ratio of drop weight mass to beam mass may also have a significant influence on the impact force profile. Although various impact force profiles have been reported by different researchers, there is no systematic study regarding the influences of the test setup on the measured impact forces. Therefore, this study numerically investigates the influences of test setups on impact force measurement and impact force profile of RC beam under drop weight impact. It is found that when the load cell is embedded into drop weight, the mass distribution of drop weight results in the measured impact force different from the actual contact force acting on the beam. On the other hand, placing load cell between drop weight and beam changes the local contact stiffness of impact zone and thus affects the impact

force profile. Different mass ratios affect the relative velocity between drop weight and beam after the first impulse and hence result in different impact force profiles.

Keywords: Drop weight; Load cell; Mass ratio; Impact force profile; RC beam

1. Introduction

Drop weight impact test is a widely used approach to study impact behavior of RC beams [1-5]. In these tests, RC beams are impacted by a drop weight falling from a certain height according to the desired impact velocity. The impact force, reaction force and midspan displacement are commonly recorded to analyse the dynamic responses of specimens. The drop weight test setups used in the previous studies of RC beams by different researchers have different configurations, which affect the test observations. For example, a previous study investigated the influences of inclination of drop weight, geometry of drop weight head, and impact interlayer on the test data [6]. It was found that these factors affected the peak impact force, impact duration, reaction force, and beam failure modes because drop weight inclination angle and head geometry affect the contact of the drop weight and RC beams. Similarly, placing a different impact interlayer such as steel plate and rubber pad between drop weight and RC beam affects the contact stiffness hence also leads to different peak impact force profiles onto RC beams. Therefore, it was concluded that careful analyses are needed when designing the drop weight test and analysing the test data to achieve the desired scenario and obtain reliable test data [6].

In addition to the influences of drop weight head geometry and impact interlayer, other factors may also affect the test results. In the drop weight impact test results reported in literature, the methods of measuring the impact force in different tests are not necessarily the same, which could affected the measurement accuracy. These measurement setups can be generally classified into two types, i.e., indirect method and direct method as shown in Fig. 1. One of the indirect methods is to calculate the impact force via multiplying the acceleration by the mass of drop weight based on Newton's Second Law. The acceleration of drop weight is obtained by attaching accelerometers to drop weight [7-9] or by differentiating the velocity of drop weight measured by laser Doppler velocimeter (LDV) system [10, 11]. Another indirect method is to sum the reaction force at the supports and the integration of the acceleration and mass of specimen along its length [8, 12]. The measurement of impact force by the indirect methods depends on the accuracy of acceleration and velocity measurement. Most impact tests adopt the direct measurement method [1, 3-5, 13, 14], in which the impact force is recorded directly by a dynamic load cell (strain gauge type [15-17] or piezoelectric type [18, 19]) mounted at the rear of drop weight head [3, 14, 20, 21] or placed between the drop weight and tested specimen [5, 22, 23] as shown in Fig 1. Obviously, the impact force acting on the tested specimens is different from the impact force recorded by the load cell installed at the rear of the drop weight head. That is, the impact force measured by the load cell would be lower than the actual contact force on the tested specimen due to the inertia force of the drop weight head. On the other hand, inserting a load cell between the drop weight and tested specimen changes the contact stiffness of impact zone, which, like placing an interlayer between the drop weight and beam, would result in different impact force profiles as reported in Ref. [6]. Therefore, different setups of load cell measurement affect the value of impact force, and those reported in literature were not necessarily the actual impact force acting on the tested RC beams. Since the impact force acting on RC beam determines the dynamic response of the tested specimen, an accurate measurement of impact force is essential to reflect the capacity of the RC beam. In addition, the accurate impact force is also important for numerical model calibration. The difference between impact force recorded by load cell and the actual contact force acting on specimens would mislead the development of reliable numerical models. To date, although the load cell has been widely used in drop weight impact test, the investigations about the effects of the mass distribution of drop weight and the load cell location on impact force are very limited. More studies about the influences of impact test configurations on accuracy of impact force measurements are deemed necessary.

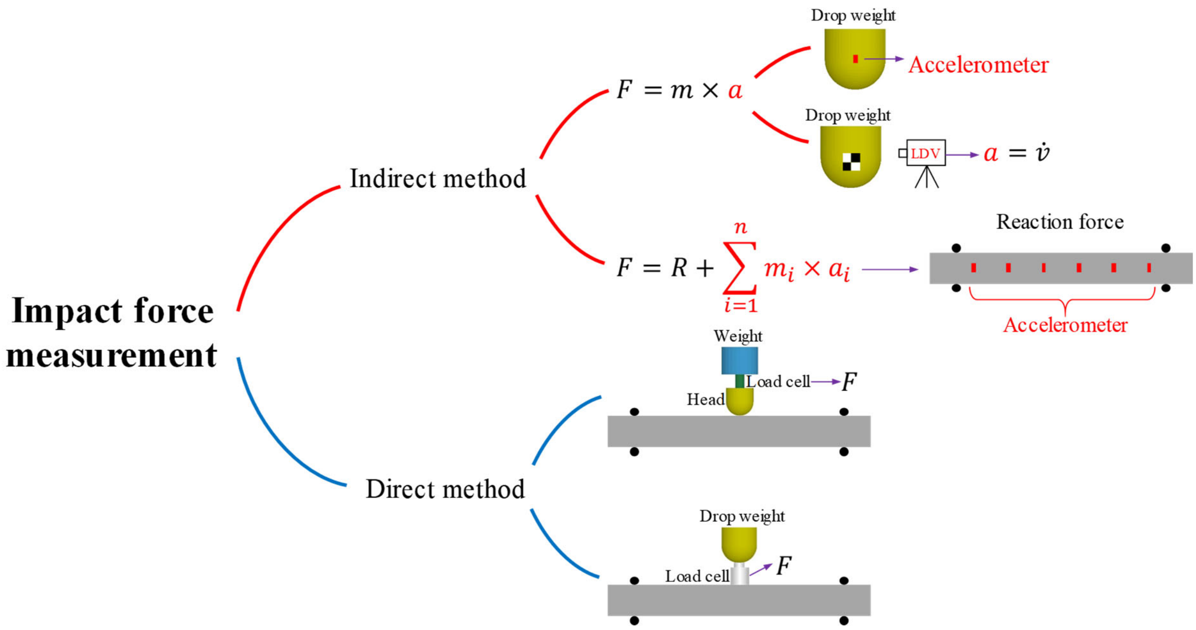

Fig. 1. Measurement methods of impact force in previous impact tests [1, 3-5, 7-14, 20-23].

Various profiles of impact force time history of RC beams under drop weight impact have been observed in the previous studies. Based on intensive literature review, the impact force profiles can be generally categorized into three types (Type I to III) based on their characteristics as shown in Fig. 2. Type I is the impact force profile with only one primary force peak [24]. Type II has a primary impact force peak followed by multiple secondary peaks [2, 7, 14, 25, 26]. The secondary force peaks gradually decrease with time. Type III has a primary impact force peak followed by a plateau [3, 4]. Type III impact force profile was observed on the RC beams [3, 4], RC columns [27] and concrete-filled steel tube columns [28, 29] in drop weight impact tests. By comparing and analysing the existing drop weight testing data of RC beam [2-4, 14, 24, 30, 31] as summarized in Table 1, it is found that the impact force profile of type I and type II were observed when the impact mass was lower than the mass of impacted specimen, while the impact force profile type III occurred when the tested specimen was impacted by a drop weight heavier than the specimen. Therefore, the mass ratio between the drop weight and the impacted specimen affects the impact force profile. However, most of the previous studies on RC beams focus on the effect of drop weight mass on the peak impact force [32, 33] instead of the entire impact force profile. It is well known that increasing the impact mass results in a higher peak impact force due to the increase of input impact energy. However, there is very limited study on how the mass ratio affects the impact force profile. The impact force profile is important as it can quantify the impulse onto the specimen and determine the specimen dynamic responses.

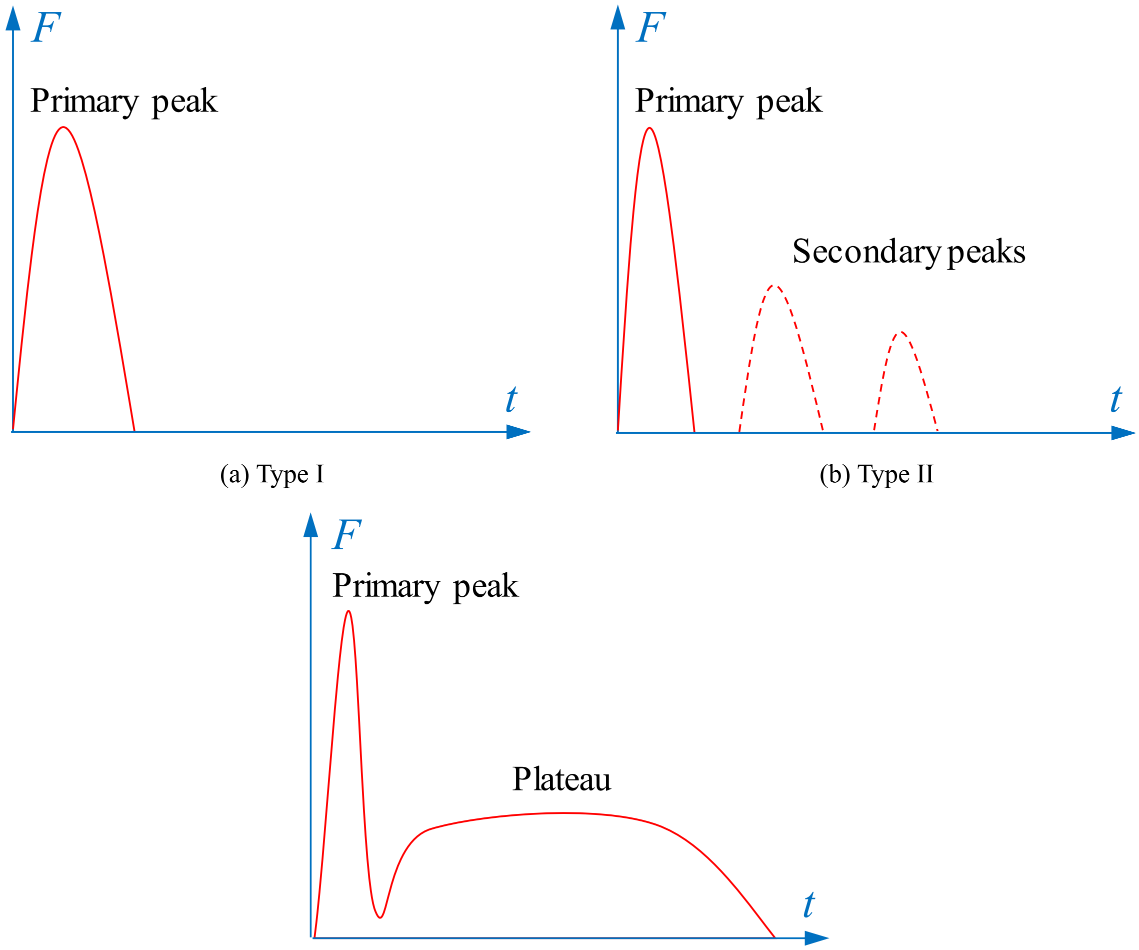

(a) Type I (b) Type II

(c) Type III

Fig. 2. Different impact force profiles of RC beam under drop weight impact.

Table 1. Summary of impact force profile type in previous drop weight impact tests of RC beam.

Reference	Specimen	Mass ratio	Impact force profile type
Chen and May, 2009 [2]	A1	0.726	Type II
	A2	0.726	Type III
	A3	1.307	Type III
	B1	0.726	Type II
	B2	1.307	Type III
	B3	0.726	Type II
	B4	1.307	Type III
Fujikake et al., 2009 [3]	S1616	3.05	Type III
	S2222	3.05	Type III
	S1322	3.05	Type III
Xu and Zeng, 2014 [30]	BD1-1	1.17	Type III
	BD2-1	1.17	Type III
	BD3	1.17	Type III
	BD4	2.67	Type III
	BD5-1	2.67	Type III

Yilmaz et al., 2014 [24]	S1	0.16	Type I
	S2	0.16	Type I
	S3	0.16	Type I
	S4	0.16	Type I
	S5	0.16	Type I
Zhao et al. 2017 [4]	B-1700-4.6	1.42	Type III
	B-1052-6.4	0.875	Type III
	B-868-7.14	0.723	Type II
	C-1700-4.6	2.36	Type III
	C-1300-5.56	1.81	Type III
	C-868-7.14	1.21	Type III
	D-1700-4.6	2.36	Type III
	D1300-5.56	1.81	Type III
	D-868-7.14	1.21	Type III
Yan et al., 2018 [14]	B1a	0.45	Type II
	B1b	0.45	Type II
Guo et al. 2019 [31]	S5	2.67	Type III
	S6	2.67	Type III
	S7	2.67	Type III
	S8	2.67	Type III

This study numerically investigates the influences of different impact test setups and the effect of mass ratio of drop weight to beam on the impact force profile and its measurement accuracy in drop weight impact tests. The accuracy of impact force measurement is quantified by comparing the contact force between drop weight and beam and the impact force measured by the load cell obtained in numerical simulations. In addition, simulations are also carried out to examine the mass ratio of drop weight to the beam on the impact force profiles.

2. Numerical model calibration

2.1. Drop weight impact test

Without loss of generality, the drop weight impact test of RC beams conducted by Fujikake et al. [3] is employed to calibrate the numerical model in this study. This experimental study reports detailed testing data and has been used for the calibration of numerical models [32, 34-37]. Fig. 3 shows the drop weight impact test setup. The RC beam is simply supported at both ends over a clear span of 1.4 m. The RC beam is impacted by a drop hammer with hemispherical head falling from various heights, i.e., 0.15 m, 0.3 m, 0.6 m, and 1.2 m. The impact force is recorded by the load cell installed at the rear of the drop weight head. The total mass of drop hammer is 400 kg. A laser displacement sensor is located below the RC beam to measure the midspan displacement. The dimension and rebar configuration of RC beam are illustrated in Fig. 4. The total length of the beam is 1.7 m. The width and depth of the beam section are 150 mm and 250 mm, respectively. A total of four longitudinal rebars with a diameter of 16 mm are placed symmetrically at the compressive and tensile sides. The 10 mm-diameter stirrups are arranged along the beam length at a space of 75 mm. The yield strength of longitudinal rebar and stirrups is 426 MPa and 295 MPa, respectively. The compressive strength of concrete is 42.0 MPa.

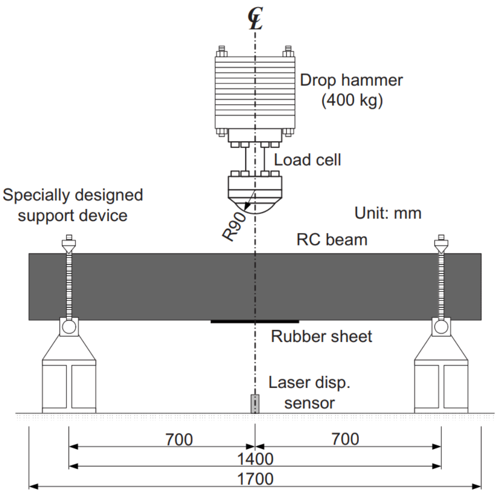

Fig. 3. Drop weight test setup (unit: mm) [3].

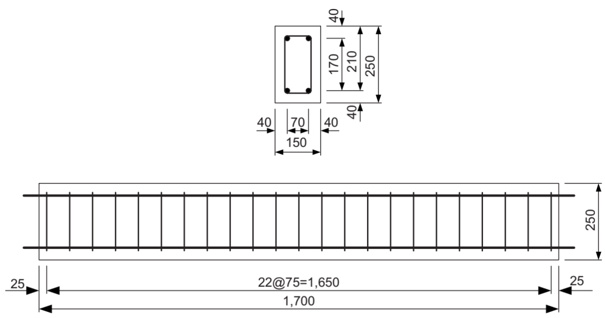

Fig. 4. Dimension and rebar configuration of RC beam (unit: mm) [3].

2.2. Numerical model

Numerical models of RC beam under drop weight impact are developed and calibrated in LS-DYNA based on the testing data [3] as shown in Fig. 5. The constant stress solid element with a single integration point is used for the concrete and drop weight. Longitudinal rebars and stirrups are simulated by Hughes-Liu beam element with 2 × 2 Gauss quadrature integration. The radius of hemispherical head of drop weight is set as 90 mm according to the test setup. Different impact velocities are assigned to the drop weight by using the keyword *INITIAL_VELOCITY_GENERATION according to the corresponding falling height. The acceleration of gravitation is set as 9.8 m/s^2 by using the keyword *LOAD_BODY. The mesh size of 10 mm for the numerical model is adopted after conducting a mesh convergence study to obtain reliable results with reasonable computational efficiency.

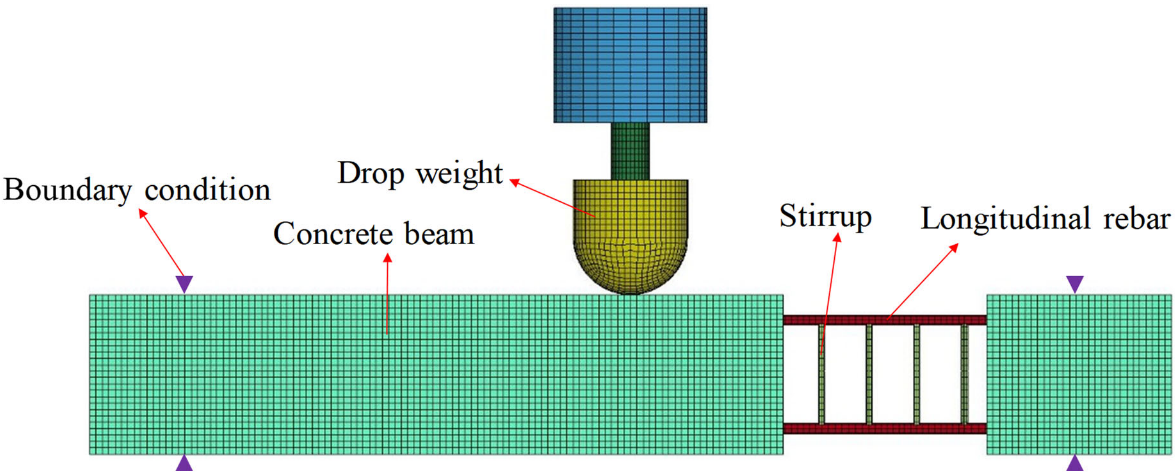

Fig. 5. Numerical model of RC beam.

2.2.1. Material model

The concrete material is simulated by *MAT_CONCRETE_DAMAGE_REL3 (MAT_72R3) in which material parameters can be generated automatically by determining the unconfined compressive strength of concrete and unit conversion factors. The concrete model has been proven able to accurately predict the dynamic behavior of RC structures under extreme dynamic loads [36, 38, 39]. Moreover, the dynamic increase factor (DIF) for concrete compressive and tensile strength [40] are employed. The keyword *MAT_ADD_EROSION is used along with the concrete model MAT_72R3 to delete over distorted concrete elements. The maximum principal strain criterion has been employed in RC structures under extreme loads in the previous studies [41-43] and it is also adopted and determined as 0.2 in this study.

The keyword *MAT_PIECEWISE_LINEAR_PLASTICITY (MAT_24) is employed for the steel longitudinal rebars and stirrups. The DIF for steel rebars proposed by Malvar [44] is defined by the keyword *DEFINE_CURVE and combined with MAT_24 model. The failure strain of steel is determined as 0.12. In addition, the elastic material model *MAT_ELASTIC (MAT_1) is used for drop weight.

2.2.2. Contact and boundary constraint

The surface to surface contact is defined between drop weight and concrete beam and the standard penalty formulation is employed (SOFT = 0) [45]. The contact stiffness scale factors (SFS/SFM) for master and slave elements are determined as 0.2. Moreover, the beam is constrained at both ends to achieve the simply supported boundary conditions by using the keyword * BOUNDARY_SPC_SET. The degrees of freedom of nodes in the boundary sets are defined to prevent the vertical movement of beam but allow free rotation of beam ends. In addition, the rebars are embedded into concrete by using the keyword

*CONSTRAINED_BEAM_IN_SOLID (CBIS).

2.2.3 Comparisons between numerical and test results

The failure modes and dynamic responses of RC beams are compared between numerical and test results as shown in Fig. 6 and Fig. 7, respectively. Accurately predicting the concrete cracks is still a challenge for researchers [46, 47]. In this numerical, the concrete cracks are presented by the numerical damage contours [32, 35]. It can be observed from Fig. 6 that the numerical concrete damage contours agree well with the concrete cracks in the test results. Vertical cracks at midspan extended from the bottom surface of beams to the impact zone are well predicted in the numerical models. With the increase of drop height, some inclined cracks appear in both the test and numerical results. Moreover, the beam impacted by the drop weight falling from a height of 1.2 m suffers a severe local concrete spalling at the side of impact zone, which is well captured in the numerical model as presented in Fig. 6. In addition, the time histories of impact force and midspan displacement are illustrated in Fig. 7. The impact force in the numerical model is consistent with that in the test result. The impact force plateau can be also seen in the numerical impact force profile. Moreover, the maximum displacement in the numerical models is comparable to the experimental maximum displacement response. These comparisons demonstrate the reliability of the numerical model, which can be used in the subsequent numerical studies about the RC beams under drop weight impact.

0.15 m

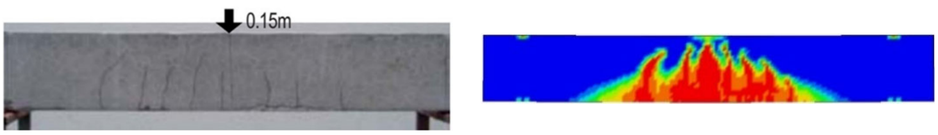

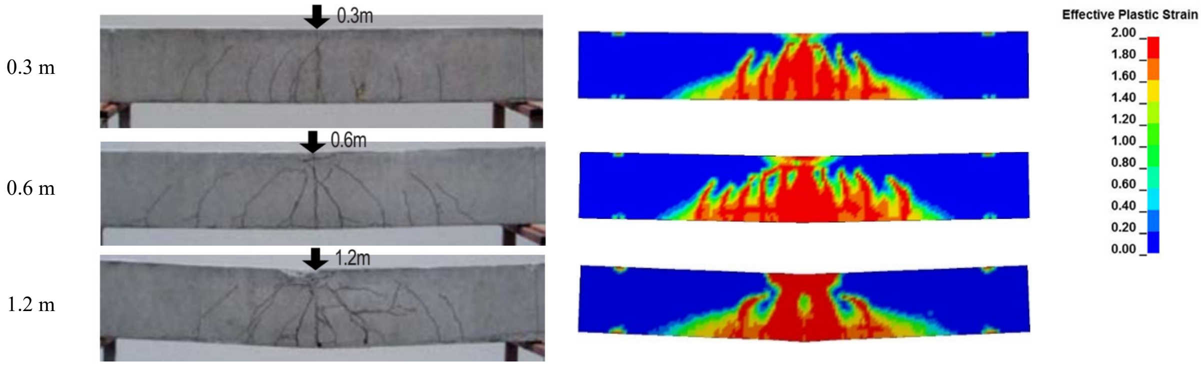

Fig. 6. Comparison of failure modes between experimental and numerical results.

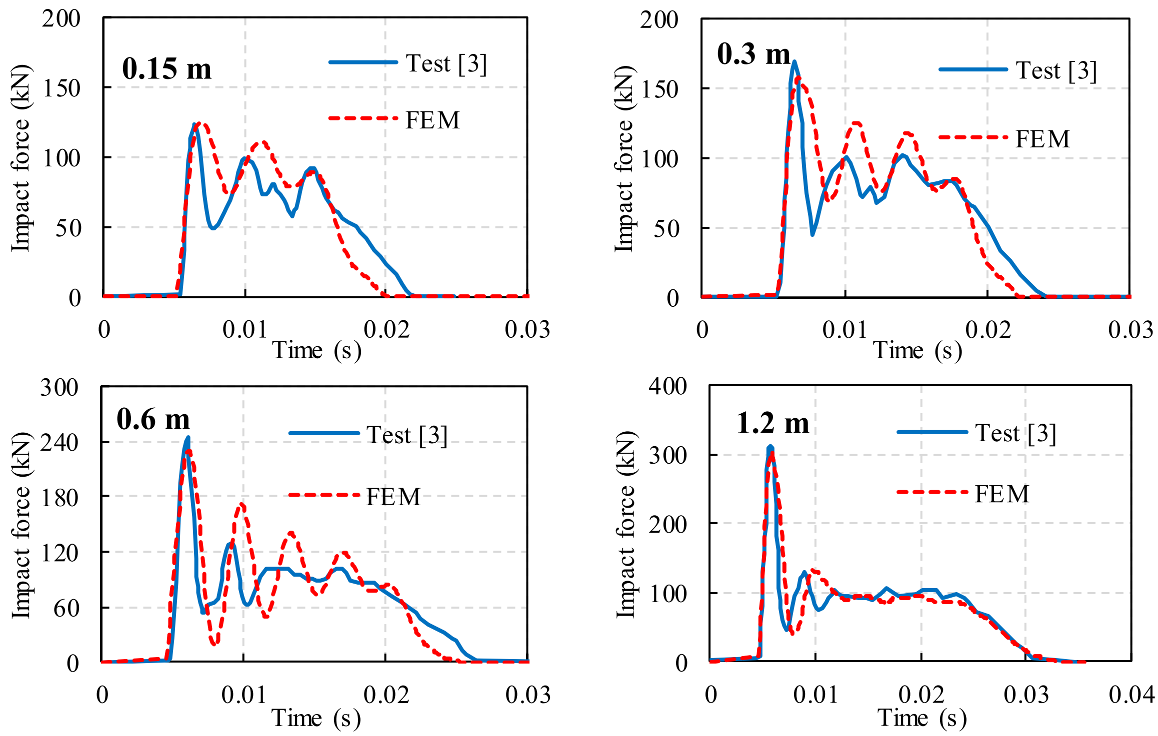

(a) Time history of impact force

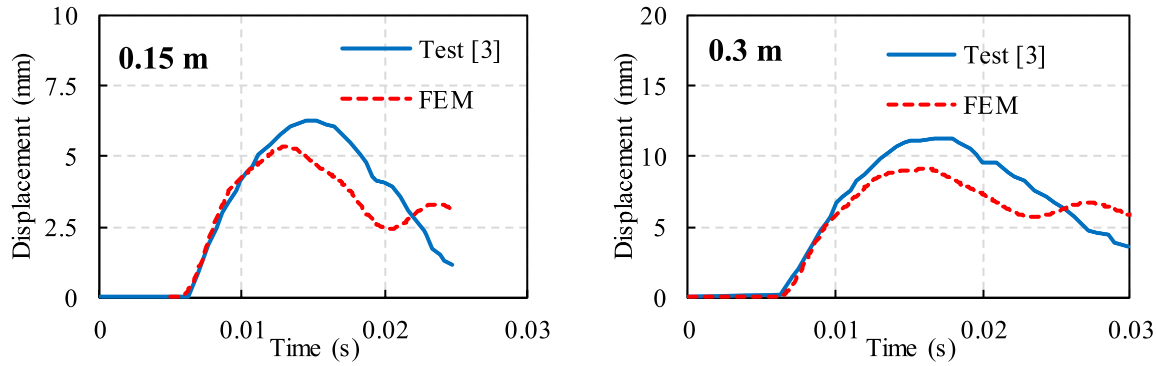

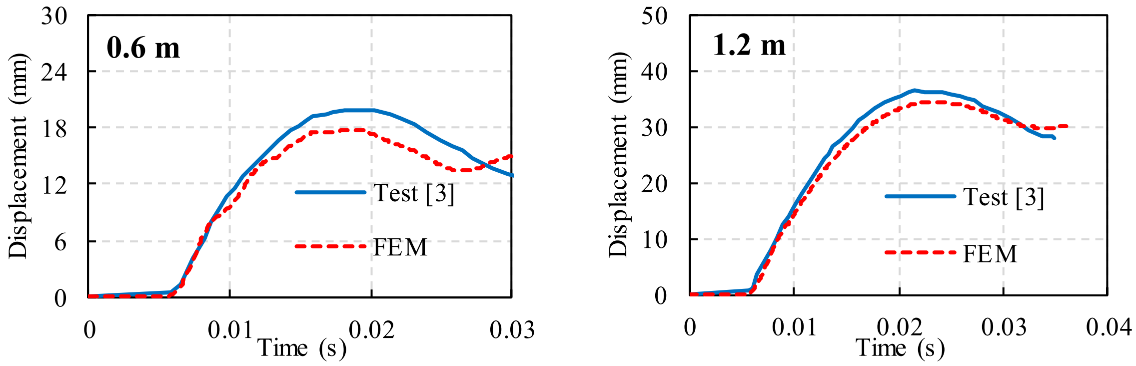

(b) Time history of displacement

Fig. 7. Comparisons of time histories of impact force and displacement between numerical and test results.

3. Impact force measurement

Load cells have been widely used in the drop weight impact test to measure the impact force. As reviewed above, the load cell can be mounted at the rear of drop weight head or placed between drop weight and beam. In this section, the influences of drop weight mass distribution and load cell location on the impact force measurement are investigated. The drop weight configuration, geometry and reinforcement layout of RC beam are kept the same as those presented in Fig. 3 and Fig. 4.

3.1. Effect of drop weight mass distribution

When the load cell is installed at the rear of the drop weight head as illustrated in Fig. 8, the mass distribution of drop weight may affect the recorded impact force. In order to investigate the effect of drop weight mass distribution on the measured impact force, the drop weight mass ratio α_d is defined as the ratio of the mass of weight above the load cell (m_w) to the mass of drop weight head (m_h), as expressed in Eq. (1).

$$\alpha_{\mathrm{d}} = \frac{m_{\mathrm{w}}}{m_{\mathrm{h}}} \tag{1}$$

Different drop weight mass ratios of 0.33, 0.5, 1.0, 2.0, 3.0, 5.0, 10.0, 20.0, 30.0, and 50.0

are employed in the study. In the simulation, the mass ratio of drop weight is adjusted by modifying the density of the weight above the load cell and the head below the load cell. It is worth mentioning that the total mass of the drop weight is kept as 400 kg and the impact velocity is 4.85 m/s. The measured dynamic force in the load cell is obtained from the axial force at the middle height of load cell in the numerical model and is defined as the impact force as illustrated in Fig. 8. The dynamic force between the drop weight and beam is identified as contact force and is compared with the impact force measured by the load cell. Fig. 9 compares the time histories of contact force and measured impact force. The overall profiles of measured impact force and contact force are similar, that is, the peak impact force is followed by a force plateau. However, it can be seen that there are some discrepancies between the contact force and the measured impact force of the specimens impacted by the drop weight when the mass ratios are low. The impact force measured by load cell is lower than the contact force directly acting on the beam. With the increase of drop weight mass ratio, the discrepancy becomes smaller and the measured impact force closes to its corresponding contact force. This can be explained by the force equilibrium according to the D'Alembert's principle as shown in Fig. 8. During the course of impact, the impact force measured by load cell (F_{lc}) is equal to the inertia force of weight (F_{iw}) which depends on the mass of weight above the load cell. F_{lc} is also equal to the subtraction of inertia force of head (F_{ih}) from contact force (F_{c}). Therefore, the contact force (F_{c}) is higher than the measured impact force (F_{lc}) from load cell. As each specimen is subjected to the identical impact mass and velocity of drop weight, each specimen has very similar contact force as shown in Fig. 9. That is to say, the mass distribution does not affect the contact force acting on the specimens but the measured impact force is affected by the mass distribution.

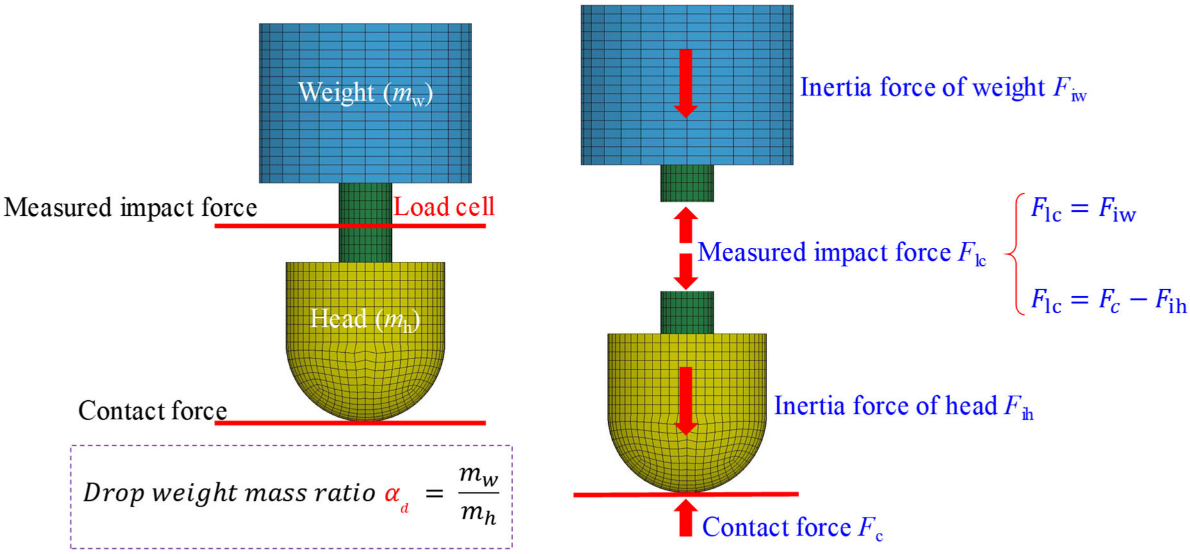

Fig. 8. Illustration of drop weight mass ratio and force equilibrium analysis.

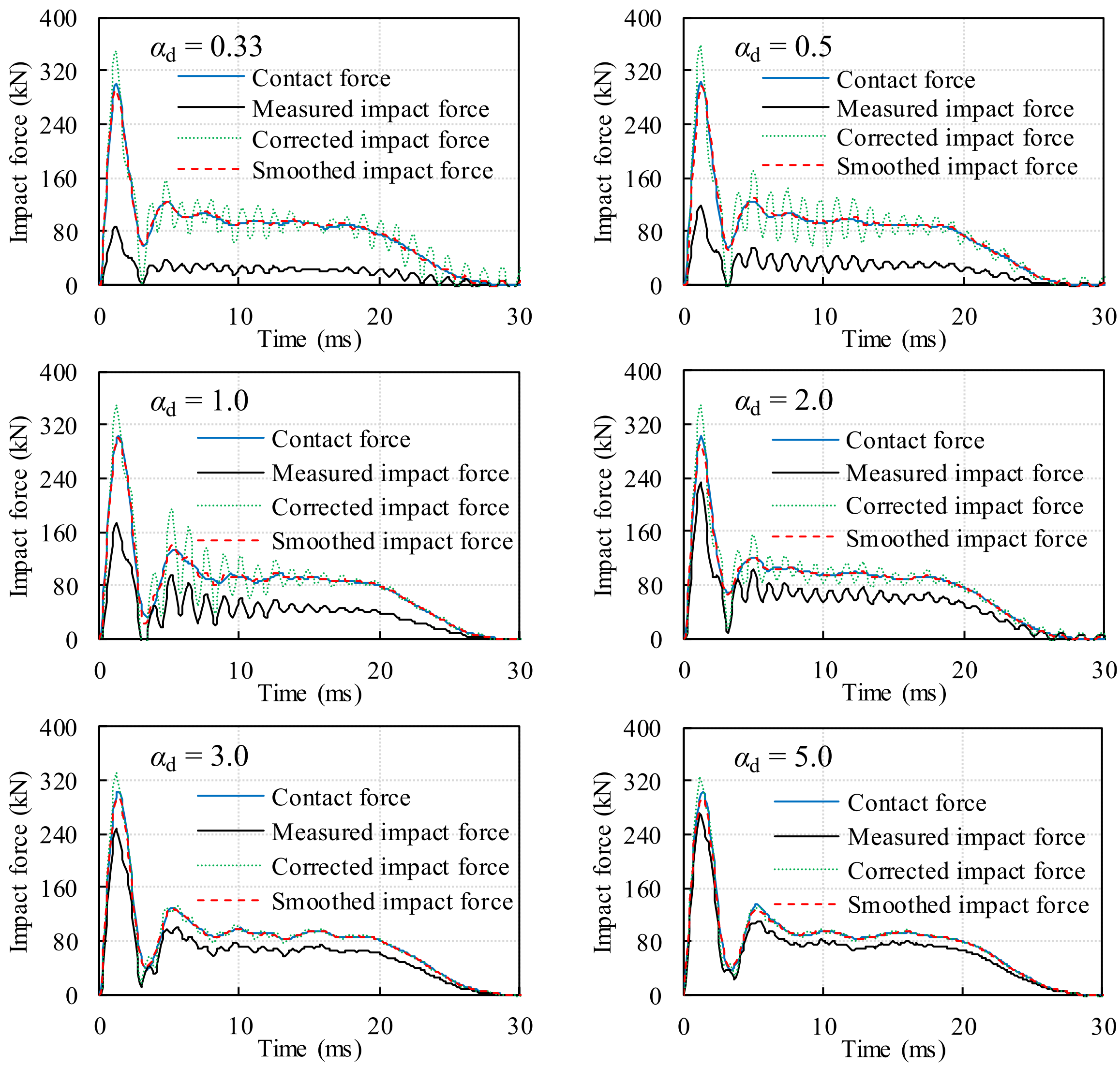

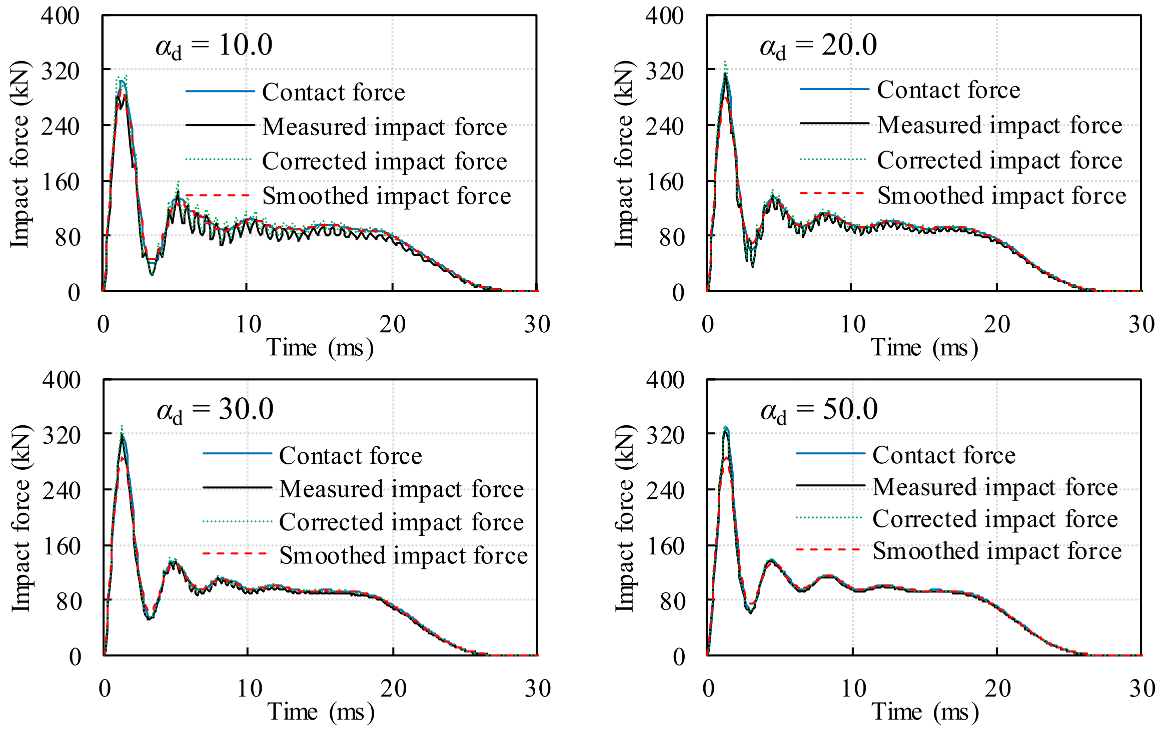

Fig. 9. Comparison between contact force and impact force.

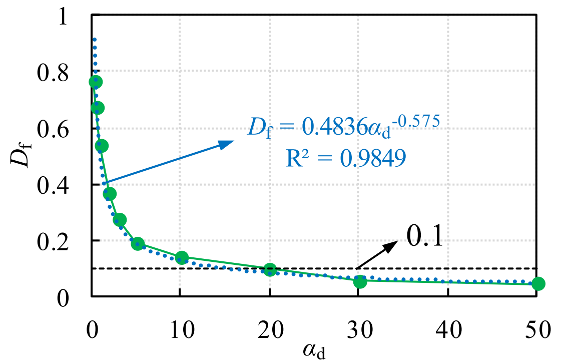

Fig. 10. The relationship between drop weight mass ratio and discrepancy of force D_f.

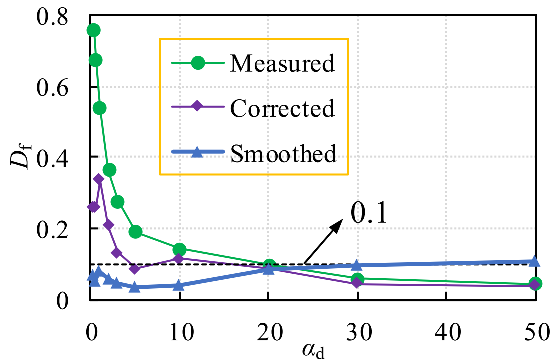

Fig. 11. D_f of measured impact force, corrected impact force and smoothed impact force.

The discrepancy between contact force and impact force (D_f) in each group as presented in Fig. 9 is assessed by the root mean square error (RMSE) as illustrated in Eq. (2).

$$D_f = \sqrt{\frac{1}{n}\sum_{i=1}^{n}\left(\frac{F_{c,i} - F_{lc,i}}{F_{c,i}}\right)^2} \quad (2)$$

where $F_{c,i}$ is the actual contact force acting on the specimen and $F_{lc,i}$ is the impact force measured by load cell at the corresponding i^{th} instant as shown in Fig. 8. The D_f of each group with different drop weight mass ratios is presented in Fig. 10. When the drop weight mass ratio is not higher than 1.0, i.e., the mass of weight is not larger than that of head, D_f is 0.76, 0.67, and 0.54 for the drop weight mass ratio of 0.33, 0.5, and 1.0, respectively. The values of D_f are higher than 0.5, indicating a larger discrepancy between the contact force and impact force. With the increase of the drop weight mass ratio, D_f decreases significantly. When the drop weight mass ratio is higher than 20.0, D_f gradually reduces to be lower than 0.1, which indicates the impact force curve agrees well with the contact force curve as shown in Fig 9. Therefore, when the drop weight mass ratio is higher than 20.0, the impact force measured by load cell is deemed accurate enough with an accumulated error less than 10% as compared to the contact force applied onto the specimen. An equation showing the relationship between the drop weight mass ratio (α_d) and D_f is proposed via the regression analysis in Eq. (3) (R^2 = 0.9849).

$$D_{\mathrm{f}} = 0.4836\alpha_{\mathrm{d}}^{-0.575} \tag{3}$$

Therefore, in the drop weight impact test, the discrepancy between the measured impact force by load cell and the actual contact force acting on the specimen can be assessed by using Eq. (3) based on the drop weight mass ratio α_d.

In addition, the impact force measured by load cell could be corrected to get better measurement of the actual impact force acting on the beam according to the drop weight mass ratio. The commonly used load cell in drop weight impact test is composed of a steel cylinder attached with several strain gauges and the steel cylinder works in an elastic state. Therefore, the drop weight with the embedded load cell can be simplified as a mass-spring system in Fig.12 based on the force equilibrium as illustrated in Fig. 8. The weight and head of drop weight are illustrated by two mass blocks. The load cell is presented by the spring with elastic stiffness k as shown in Fig. 12 and thus the spring force is the measured impact force in load cell. According to the D'Alembert's principle, the dynamic equilibrium equations are expressed as follows

$$m_{\mathrm{w}}\ddot{x}_{\mathrm{w}} - k(x_{\mathrm{w}} - x_{\mathrm{h}}) = 0 \tag{4}$$

$$m_{\mathrm{h}}\ddot{x}_{\mathrm{h}} + k(x_{\mathrm{w}} - x_{\mathrm{h}}) = F_{\mathrm{c}}(t) \tag{5}$$

where x_{w} and x_{h} are the vertical displacement of weight and head, while $\ddot{x}_{\mathrm{w}}$ and $\ddot{x}_{\mathrm{h}}$ are the acceleration of weight and head. F_{c}(t) is the time history of contact force between drop weight and RC beam. The accelerations of drop weight head ($\ddot{x}_{\mathrm{h}}$) and weight above the load cell ($\ddot{x}_{\mathrm{w}}$) are deemed as identical because the drop weight impact of concrete specimen is hard impact. Therefore,

$$\ddot{x}_{\mathrm{w}} = \ddot{x}_{\mathrm{h}} = \frac{F_{\mathrm{c}}(t)}{m_{\mathrm{w}} + m_{\mathrm{h}}} \tag{6}$$

The measured impact force F_{lc}(t) in load cell illustrated by the spring force is given by

$$F_{\mathrm{lc}}(t) = k(x_{\mathrm{w}} - x_{\mathrm{h}}) = m_{\mathrm{w}}\ddot{x}_{\mathrm{w}} = \frac{m_{\mathrm{w}}}{m_{\mathrm{w}} + m_{\mathrm{h}}} F_{\mathrm{c}}(t) \tag{7}$$

When the mass ratio of drop weight in Eq. (1) is introduced into Eq. (7), the relationship between the actual contact force and the measured impact force is found to be

$$F_{\mathrm{c}}(t) = (1 + \frac{1}{\alpha_{\mathrm{d}}})F_{\mathrm{lc}}(t) \tag{8}$$

Thus, the impact force correction factor β_{c} can be expressed as follows.

$$\beta_{\mathrm{c}} = 1 + \frac{1}{\alpha_{\mathrm{d}}} \tag{9}$$

The measured impact force in load cell can be corrected by multiplying the correction factor β_{c} to obtain the actual contact force. The corrected impact force is also presented in Fig. 9. It can be seen that the corrected impact force is close to the actual contact force by amplifying the measured impact force with the correction factor β_{c}. Fig. 11 compares D_{f} of the original impact force and the corrected impact force. D_{f} of the corrected impact force is calculated according to the RMSE of the actual contact force and the corrected impact force. As shown in Fig. 11, D_{f} of the corrected impact force is lower than that of original impact force for all specimens, indicating a smaller discrepancy between the corrected impact force and the actual contact force.

However, the D_f of the corrected impact force in most cases is still higher than the expected threshold of 0.1 and there are still some discrepancies at the peak impact force, owing to the significant fluctuations in the measured impact force in load cell.

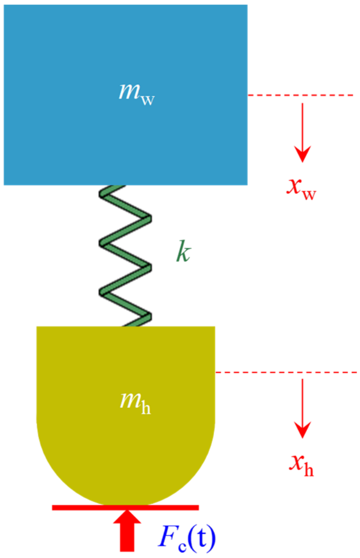

Fig. 12. Simplified mass-spring system for drop weight.

For the simplified mass-spring system of drop weight as shown in Fig. 12, varying the mass ratio of drop weight changes the mass distribution of the mass-spring system and thus causes the variation of the natural frequency of the system. The natural frequency of the system is given as follows,

$$\omega = \sqrt{\frac{k(m_w + m_h)}{m_w \cdot m_h}} \tag{10}$$

In this study, the mass of drop weight $(m_w + m_h)$ is kept as a constant of 400 kg and the spring stiffness for load cell is also constant. By normalizing the spring stiffness k and the mass of whole drop weight as 1, the relationship of ω and m_h can be derived as,

$$\omega = \sqrt{\frac{1}{m_h \cdot (1 - m_h)}} \tag{11}$$

and the period of the mass-spring system is

$$T = 2\pi\sqrt{m_h \cdot (1 - m_h)} \tag{12}$$

The relationship between the period of the system and m_h is illustrated in Fig. 13. It is found that the period of system is the largest when m_h is 0.5, i.e. drop weight mass ratio $\alpha_d = 1.0$. The period of system becomes shorter for other mass ratios. Since the contact force acting on the mass-spring system is identical in all the specimens with different drop weight mass ratios, the system with the longest period (mass ratio $\alpha_d = 1.0$) would lead to the largest spring response, which causes the largest fluctuation between the measured and corrected impact forces. The difference between the corrected peak impact force and the actual peak contact force is shown in Fig. 9.

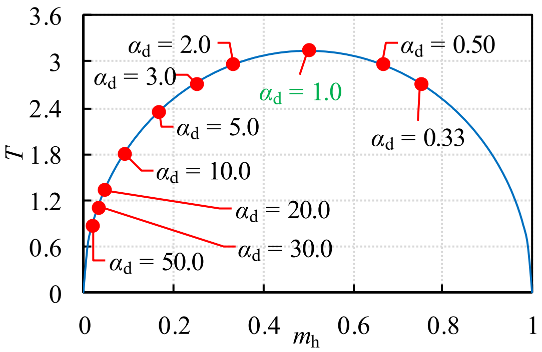

Fig. 13. Relationship between the mass of drop weight head and the period of system.

In order to obtain more accurate actual contact force, the Savitzky-Golay smoothing method is employed to reduce the fluctuation of impact force. It can be seen from Fig. 9 that the smoothed impact force in general agrees well with the actual contact force. The more accurate peak force also can be well obtained. The D_f of smoothed impact force is lower than the expected threshold of 0.1 as presented in Fig. 11. However, it is found that the smoothed peak force is lower than that of actual contact force when the mass ratio of drop weight is higher than 20.0. Since D_f of these specimens is lower than 0.1, the corrected impact force is accurate enough to represent the actual contact force. However, if the smoothing method is used for these specimens with the mass ratio higher than 20.0, the smoothed impact force would lead to a higher D_f than that of the measured and corrected impact force as shown in Fig. 11. A flowchart to obtain the actual contact force acting on beam in the drop weight impact test is presented in Fig. 14.

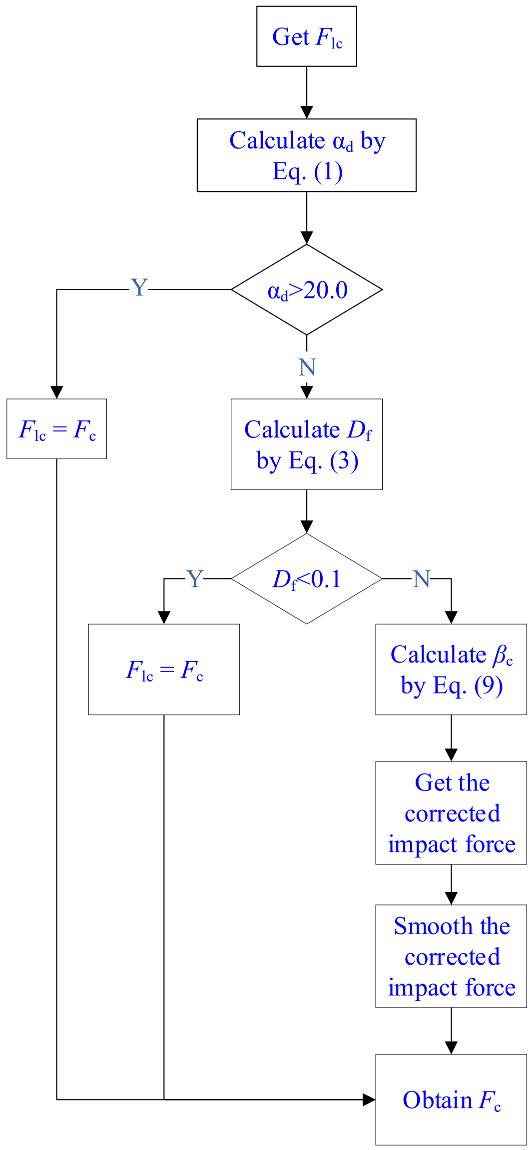

Fig. 14. Flowchart to obtain actual contact force.

To sum up, the mass distribution of drop weight has a significant effect on the accuracy of measured impact force. When the mass of drop weight head is larger than that of weight above load cell, the measured impact force deviates significantly from the actual contact force acting on the specimen. Thus, the drop weight mass ratio should be carefully designed to obtain more precise impact force in drop weight impact tests, especially in the case of drop weight with relatively small mass. The measured impact force in the load cell mounted at the rear of drop weight head is suggested to be corrected if the drop weight mass ratio is lower than 20.0. The actual force acting on beam can be obtained according to the steps in flowchart in Fig. 14. Moreover, in the numerical simulation of drop weight impact, the numerical impact force is usually determined by the contact force between the drop weight and specimen [48-50] and is compared with the measured experimental impact force in load cell. If the experimental impact force is measured by load cell mounted at the rear of drop weight head and the drop weight mass ratio is lower than 20.0, the effect of drop weight mass distribution should be also considered in the numerical model to obtain the correct impact force and accurately calibrate the numerical model.

3.2. Effect of load cell location

In addition to load cell embedded into the drop weight, load cell may be placed on the beam directly, that is, located between drop weight and impacted specimen [5, 22, 23]. The previous study reported that placing an interlayer between drop weight and beam resulted in different impact force profiles [6]. Therefore, load cell placed between drop weight and RC beam can affect the impact force profile. In this section, the effect of load cell location on the impact force acting on the RC beam is investigated. The numerical models of locating load cell at the rear of drop weight head (setup I) or between drop weight and beam (setup II) are shown in Fig. 15. The impact mass and impact velocity of drop weight are 400 kg and 4.85 m/s, respectively. Fig. 16 illustrates the shape and dimension of load cell used in the previous drop weight impact tests [5]. The mass of load cell is about 18.1 kg and the density of load cell is adjusted to match the mass of load cell. Moreover, the contact between drop weight and load cell and the contact between load cell and RC beam are defined as the surface to surface contact.

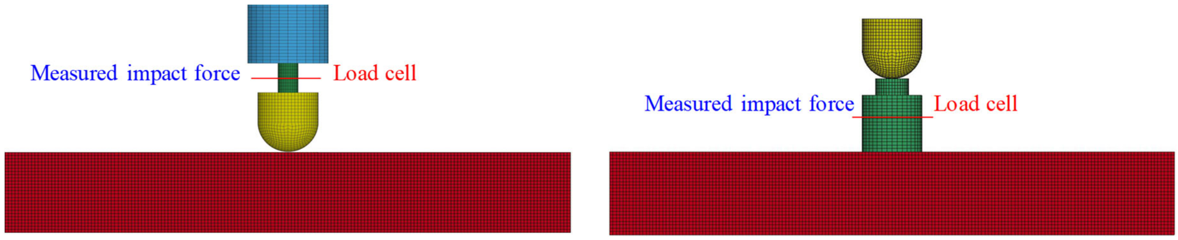

(a) Setup I: load cell mounted at the rear of drop weight head
(b) Setup II: load cell placed between drop weight and beam

Fig. 15. Different load cell locations.

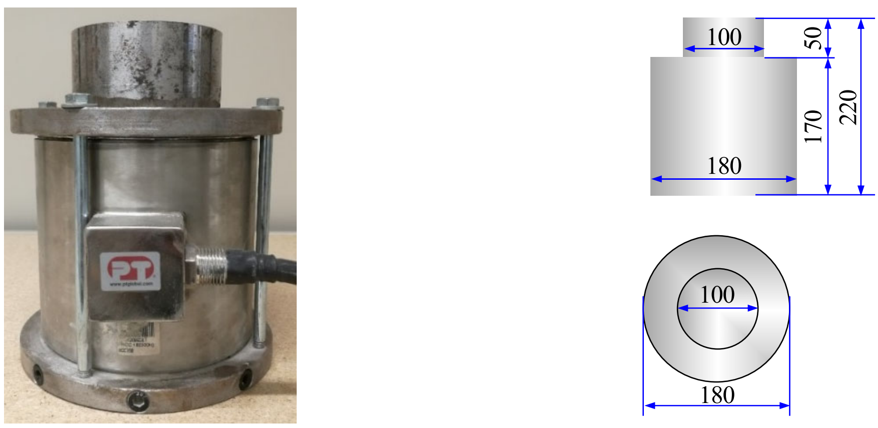

(a) Load cell used in drop weight impact test [5]
(b) Load cell dimension (unit: mm)

Fig. 16. Dimension of load cell.

In the numerical model as shown in Fig. 15(a), a drop weight with load cell mounted at the rear of drop weight head impacts the RC beam directly. As presented above, when the mass ratio is large, the mass distribution of drop weight has insignificant influence on the measurement of impact force, the drop weight mass ratio (α_d) of 50.0 is therefore adopted in this section, and the impact force measured by the embedded load cell is compared with that measured in setup II as shown in Fig. 15(b). It is worth mentioning that the measured impact force in the load cells is obtained from the section axial force at the middle height of load cells as illustrated in Fig. 15. Fig. 17(a) shows the time histories of the measured impact forces in the numerical models. During the first impact pulse, the peak impact force measured in the embedded load cell (setup I) is lower than that in the load cell placed between drop weight and beam (setup II). The impact duration of the first impulse obtained by the setup I is 3.5 ms while that of dynamic forces in the setup II is 2.4 ms. This is because the steel load cell increases the contact stiffness and leads to a higher force peak and a shorter duration. Moreover, it is worth noting that the measured impact force reaches its peak at 1.3 ms and 0.9 ms for the setup I and setup II, respectively, indicating that using steel load cell between drop weight and beam leads to a higher loading rate. In addition, a force plateau following the first impact pulse is measured by the load cell mounted at the rear of drop weight head, while multiple secondary peaks are observed by using the placed load cell. That is to say, given the same input impact energy, the force measured by the load cell in the setup I shows the impact force profile of type III, which is different from that of type II in the setup II. Therefore, placing load cell between drop weight and beam changes the local contact stiffness and thus affects the impact force profile including the primary impact pulse and the subsequent secondary force peaks or plateau.

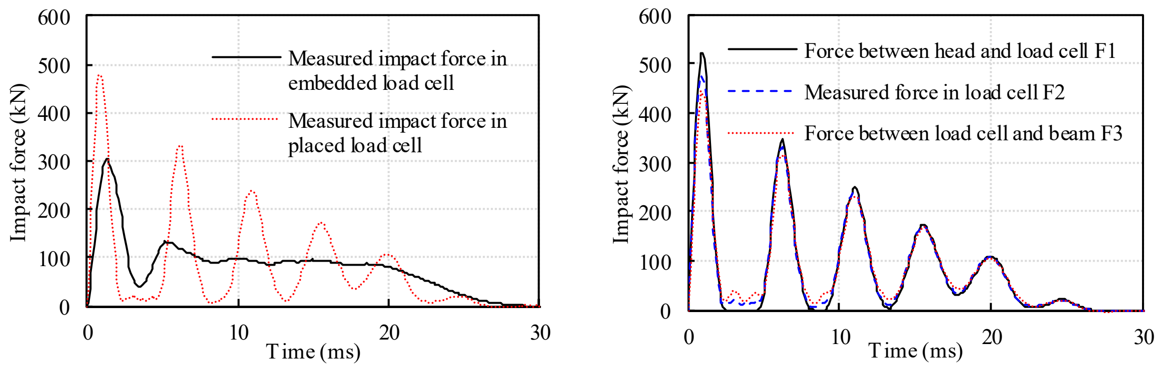

(a) Comparison of measured impact force in load cell with different locations

(b) Comparison of dynamic force in load cell placed on the beam

Fig. 17. Effect of load cell location on the impact force.

For the case with load cell being placed between drop weight and beam (setup II), three dynamic forces, i.e., the contact force between the drop weight head and load cell (F_1), the measured impact force in load cell (F_2), and the contact force between load cell and RC beam (F_3), are compared as shown in Fig. 17(b). It is found that F_1 has the highest first peak of 522.45 kN, followed by F_2 of 476.94 kN and F_3 of 443.33 kN. During the course of impact, the drop weight first contacts the load cell, which mobilizes an upwards inertia force of load cell. According to force equilibrium as shown in Fig. 18, the contact force between drop weight and load cell (F_1) is balanced by the upward inertia force and the contact force between load cell and beam (F_3). The inertia force of load cell results in a 15.14% difference between F_1 and F_3. Moreover, the impact force (F_2) measured by the load cell experiencing an upward inertia force is usually higher than the actual contact force (F_3) applied onto the beam. For example, the difference in peak impact force between the measured F_2 and F_3 acting on the beam is 7.05%. Since the load cell placed on the beam suffers an upward inertia force which is mainly governed by its weight, it is suggested to employ the load cell as light as possible in the setup II.

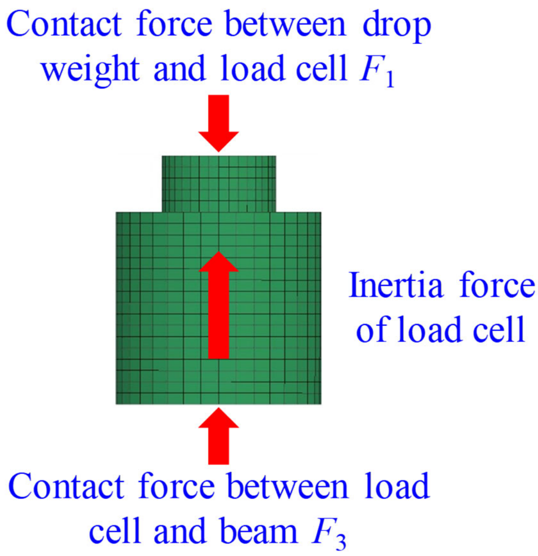

Fig. 18. Force equilibrium of load cell.

4. Effect of mass ratio

Based on the previous testing data [2-4, 7, 14, 24-26], the impact force profiles can be categorized into three types as illustrated in Fig. 2. The impact force depends on the interaction of drop weight with the beam. Upon impact, drop weight with a lighter mass would bounce off quickly from a heavier beam while a heavier drop weight would move together with a lighter beam. The masses of drop weight and beam affect the motion state of beam and drop weight and further influence the impact force profile. The mass ratio (α) is defined as,

$$\alpha = \frac{m_{\mathrm{d}}}{m_{\mathrm{b}}} \tag{13}$$

where m_d is the mass of drop weight and m_b is the mass of beam between two supports. In this study, the dimension and rebar layout are identical to those as shown in Fig. 4 and the mass of beam is kept the same as 131.25 kg. The mass of drop weight varies from 32.81 kg to 525.0 kg to have the corresponding mass ratio (α) in the range of 0.25 to 4.0. The drop weight falls from a height of 0.3 m, 0.6 m, 1.2 m or 2.4 m to reach an impact velocity of 2.42 m/s, 3.43 m/s, 4.85

m/s, or 6.86 m/s, respectively.

4.1. Numerical results with different mass ratios

Fig. 19 shows the impact force acting on beams impacted by drop weight with different mass ratios and falling from different heights. In general, increasing the mass ratio increases the first peak of impact force, impact duration of first impulse and total impact duration. For the drop weight impact with the minimum mass ratio of 0.25 at different velocities, only one primary pulse is observed in the impact force profile (Type I), indicating that the drop weight and beam separate after the impact. The drop weight rebounds upwards and the beam moves downwards. In terms of the mass ratios of 0.5, 0.75, and 1.0, the impact force profile presents a primary pulse followed by one or more secondary pulses (Type II) with the increase of mass ratio. The higher mass ratio yields more secondary pulses. This can be explained that the heavier drop weight has larger inertia and thus is more difficult to bounce off the beam, leading to an increased number of contact and impact duration. Moreover, regarding the mass ratio of 2.0, 3.0, and 4.0, a force plateau appears (Type III) after the primary impact. However, the impact force plateau presents fluctuations under the drop heights of 0.3 m and 0.6 m (relatively low impact velocity) or remains almost constant at about 100.0 kN under the drop weights of 1.2 m and 2.4 m (higher impact velocity). In addition, it is worth noting that the impact force drops to a small amplitude after the first peak as highlighted in Fig. 19(c) and (d). The small minimum force amplitude changes from zero to a certain value with the increase of mass ratio. The higher mass ratio yields a larger minimum force amplitude. For example, when the mass ratio is less than 2.0, the force drops to zero as shown in Fig. 19(c). However, the minimum force is 12. 44 kN, 39.70 kN, and 42.03 kN for the mass ratio of 2.0, 3.0, and 4.0, respectively. It can be concluded that the mass ratio has a significant effect on the impact force profile. The impact force profile with a force plateau occurs when the mass ratio is larger than 2.0. Under the same mass ratio, the lower impact velocity results in the fluctuations of force plateau while the higher impact velocity leads to an almost constant impact force plateau.

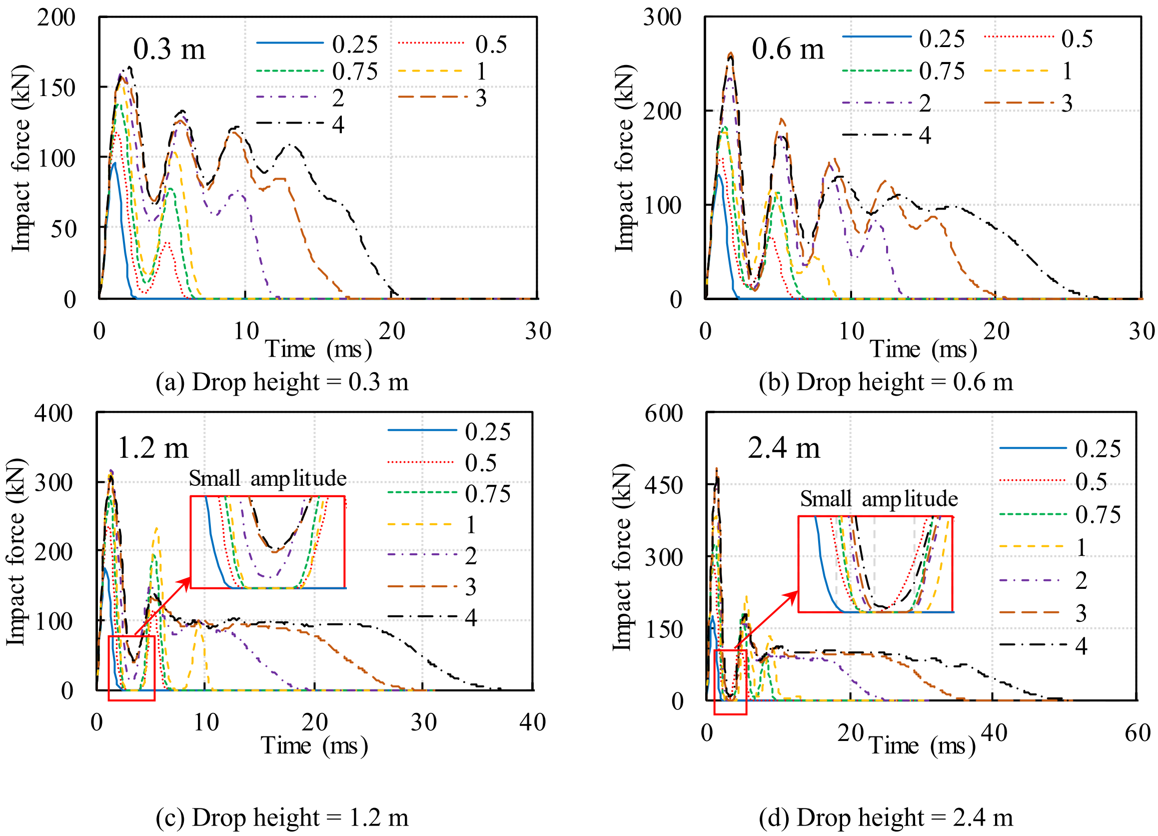

(a) Drop height = 0.3 m (b) Drop height = 0.6 m

(c) Drop height = 1.2 m (d) Drop height = 2.4 m

Fig. 19. Time history of impact force for different mass ratios.

4.2. Discussion and analysis of different impact force profiles

According to the results shown in Fig. 19, the impact force profile can be summarized as three types, i.e., only one primary force peak (Type I as shown in Fig. 2(a)), primary force peak with one or multiple secondary peaks (Type II as shown in Fig. 2(b)), and primary force peak followed by a force plateau (Type III as shown in Fig. 2(c)). In order to better demonstrate the effect of mass ratio on the motion state of drop weight and beam and on the impact force profile, the time histories of impact force, velocities of drop weight and beam, and displacements of drop weight and beam at the impact zone are presented in Fig. 20. The numerical results with the mass ratios of 0.25, 0.5 and 3.0 at the drop height of 1.2 m representing the three impact force profile types are employed for the comparison.

In terms of the mass ratio of 0.25, the impact force profile has only one pulse (type I) as presented in Fig. 20(a). During the course of impact, the displacement of drop weight is slightly larger than that of beam at the impact zone, indicating the drop weight and beam are in contact. The interaction between drop weight and beam decelerates the drop weight but accelerates the beam downwards, resulting in a decrease of drop weight velocity but an increase of beam velocity. The velocity of drop weight decreases and turns into positive (i.e., the drop weight moves upwards) as shown in Fig. 20(a) because of the upward reaction force from the beam applying on the drop weight. This leads to the separation between drop weight and beam and consequently the decrease of impact force to zero. At the end of the primary impulse, the velocity of drop weight is upward and the drop weight is separated from the beam. Therefore, it can be seen that the drop weight rebounds off the beam after the first impact, leading to only one primary force peak in the impact force profile.

For the case with mass ratio 0.5, the impact force, velocity, and displacement are illustrated in Fig. 20(b). During the first impact pulse, the changes of beam velocity and drop weight velocity as well as the impact force are similar to those for the mass ratio of 0.25. However, the velocity of drop weight at the end of primary impulse drops to about 0.22 m/s which is much lower than its initial velocity of 4.85 m/s. After the first impact pulse, the displacement of beam becomes larger than that of drop weight, which implies that the beam and the drop weight are separated. The drop weight moves downwards with the velocity of 0.22 m/s until the second impact occurs. The beam decelerates due to its flexural stiffness and reaches the maximum displacement. Then the beam moves upwards to recover its elastic deformation. The opposite movement direction of beam and drop weight results in the second impact as shown in Fig 20. This impact process may continue several times until the drop weight rebounds off the beam and the multiple secondary force peaks appear in the impact force profile type II as shown in Fig. 2.

For the case with mass ratio 3.0, the impact force profile presents a force plateau after the primary impact as shown in Fig 20(c). After the first force peak, the impact force decreases due to the reduction in the relative velocity of drop weight and beam. The impact force drops to a certain value instead of zero, implying that the drop weight and beam are still in contact and moving in the same direction. The beam accelerates to its maximum velocity of 4.69 m/s and then decelerates to the velocity of 2.99 m/s, which is close to the velocity of drop weight as shown in Fig 20(c). Then the impact force increases to a plateau with an almost constant value. The velocity of drop weight is close to that of beam during the force plateau, that is to say, the velocity difference between drop weight and beam is very small. Therefore, the beam and drop weight keep in contact and move together with a close and gradually declining velocity. When the velocity of beam and drop weight becomes zero, the initial kinetic energy of drop weight is dissipated by the elastic and plastic deformation of beam. At this instant, the displacement of beam reaches its maximum and the impact force plateau begins to decrease. Then the drop weight and beam move upwards together until the elastic deformation of beam is recovered. The velocity of beam and drop weight reaches the upward maximum. Due to the flexural stiffness of beam, the velocity of beam decreases gradually and is lower than that of drop weight. The velocity difference between beam and drop weight results in the final separation of beam and drop weight and thereby impact force drops to zero at the end of impact.

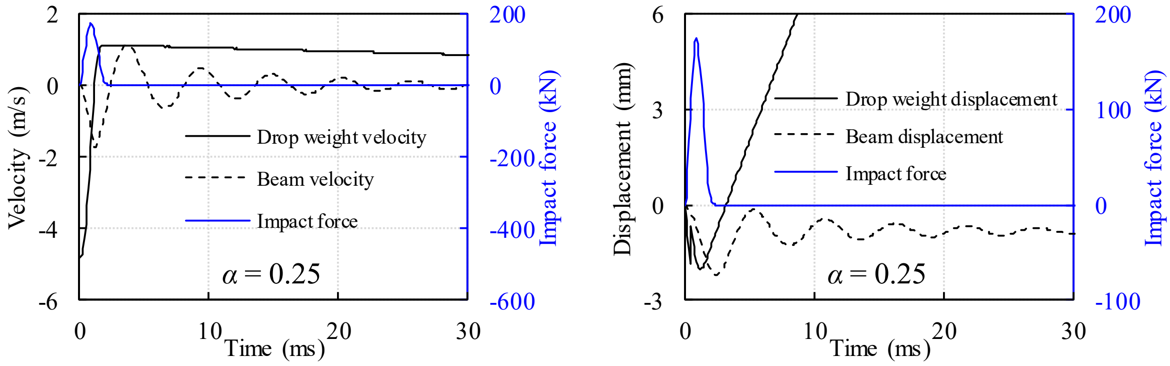

(a) Mass ratio of 0.25

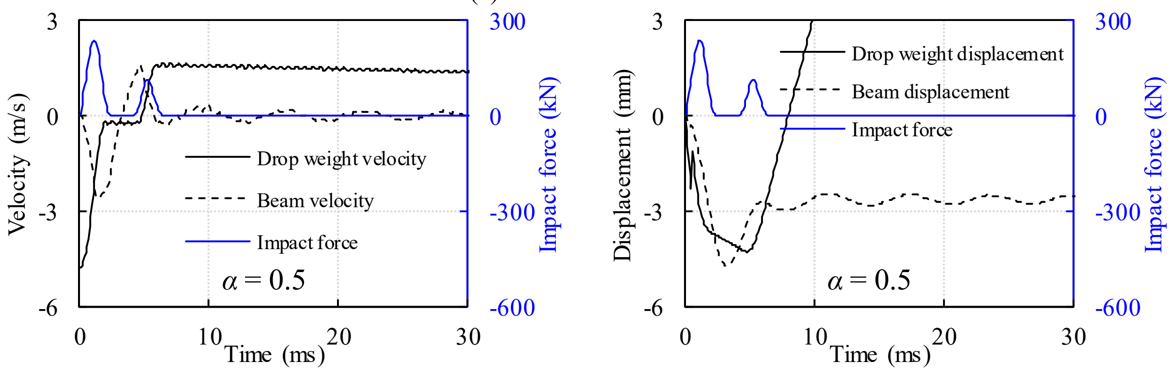

(b) Mass ratio of 0.5

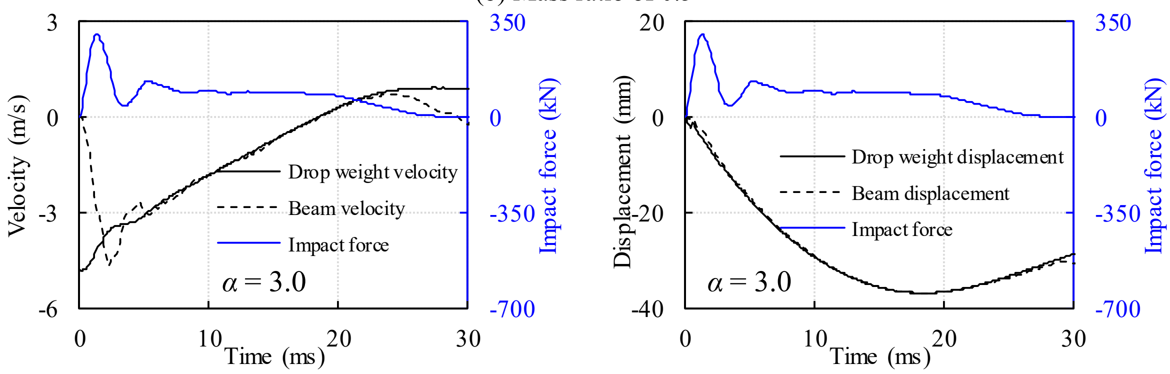

(c) Mass ratio of 3.0

Fig. 20. Time histories of impact force, velocity, and displacement.

Primary impact pulse appears in the impact force profile regardless of its type. After the primary impact pulse, the drop weight and beam with various mass ratios exhibit different velocities, which causes different interactions between drop weight and beam and thus generates various impact force profiles. In addition, the beam at midspan moves downwards and experiences a certain vertical displacement during impact. The vertical displacement mobilizes the flexural stiffness of beam which provides a certain resistance and reduces the beam velocity. The beam moves downwards to its maximum displacement. After that, the beam returns and moves upwards to recover its elastic deformation. Therefore, the flexural stiffness of beam affects the beam velocity after the first impact. In addition, the contact stiffness at the impact zone has effect on the whole impact force profile. It can be concluded that the primary impact peak is governed by the impact energy and local contact stiffness while the remaining part of impact force profile is related to other factors such as mass ratio, contact stiffness and flexural stiffness of beam.

5. Conclusions

This study investigates various impact force measurement methods and the effect of mass ratio on the impact force profile of RC beam under drop weight impact. Different mass distributions of drop weight on the measured impact force are studied to reveal their influence on the accuracy of measuring impact force. The impact forces measured by load cell mounted at the rear of drop weight head and directly placed on the beam are compared. In addition, the effect of mass ratio (α) of drop weight mass to beam mass on the impact force profile is discussed. The major conclusions drawn in this study are summarized as follows.

(1) The drop weight mass distribution has a significant effect on the measured impact force by the load cell mounted at the rear of the drop weight head. The measured impact force by load cell agrees well with the contact force when the mass ratio of weight to drop weight head (α_d) is higher than 20.0. In contrast, if the mass ratio of weight to drop weight head (α_d) is less than 20.0, the measured impact force deviates from the actual contact force acting on the beam by more than 10%. The measured impact force by load cell can be corrected by using the proposed correction method to derive more accurate contact force acting on the beam.

(2) Load cell mounting at the rear of the drop weight head or placing between the drop weight and beam results in different impact force profiles. Placing load cell between the drop weight and beam increases the local stiffness and leads to higher impact force peak, shorter duration, and multiple secondary force peaks as compared with the impact forces from load cell mounted at the rear of drop weight.

(3) The mass ratio of drop weight mass to beam mass (α) affects the relative velocity between drop weight and beam after the first impact pulse and thus influences the impact force profiles. In this study, with the mass ratio of 0.25, only one primary impact force peak (type I) can be observed in the impact force profile. For the cases with mass ratios of 0.5, 0.75, and 1.0, the impact force profile exhibits a primary impact pulse followed by one or multiple secondary pulses (type II). With the mass ratio of 2.0, 3.0, and 4.0, the impact force profile consists of a primary pulse followed by a force plateau (type III).

Acknowledgements

The authors acknowledge the financial support from the Australian Research Council (ARC) via Australian Laureate Fellowship (FL180100196). The first author also gratefully acknowledges the financial support from Curtin International Postgraduate Research Scholarship (CIPRS) and Curtin Strategic International Research Scholarship (CSIRS).

References

[1]. Kishi, N., Mikami, H., Matsuoka, K.G., and Ando, T., *Impact behavior of shear-failure-type RC beams without shear rebar.* International Journal of Impact Engineering, 2002. 27(9): 955-968.

[2]. Chen, Y. and May, I.M., *Reinforced concrete members under drop-weight impacts.* Proceedings of the Institution of Civil Engineers-Structures and Buildings, 2009. 162(1): 45-56.

[3]. Fujikake, K., Li, B., and Soeun, S., *Impact Response of Reinforced Concrete Beam and Its Analytical Evaluation.* Journal of Structural Engineering, 2009. 135(8): 938-950.

[4]. Zhao, D., Yi, W., and Kunnath, S.K., *Shear Mechanisms in Reinforced Concrete Beams under Impact Loading.* Journal of Structural Engineering, 2017. 143(9): 04017089.

[5]. Pham, T.M., Hao, Y., and Hao, H., *Sensitivity of impact behaviour of RC beams to contact stiffness.* International Journal of Impact Engineering, 2018. 112: 155-164.

[6]. Li, H., Chen, W., and Hao, H., *Influence of drop weight geometry and interlayer on impact behavior of RC beams.* International Journal of Impact Engineering, 2019. 131: 222-237.

[7]. Kishi, N. and Bhatti, A.Q., *An equivalent fracture energy concept for nonlinear dynamic response analysis of prototype RC girders subjected to falling-weight impact loading.* International Journal of Impact Engineering, 2010. 37(1): 103-113.

[8]. Huynh, L., Foster, S., Valipour, H., and Randall, R., *High strength and reactive powder concrete columns subjected to impact: Experimental investigation.* Construction and Building Materials, 2015. 78: 153-171.

[9]. Yoo, D.-Y., Banthia, N., Kim, S.-W., and Yoon, Y.-S., *Response of ultra-high-performance fiber-reinforced concrete beams with continuous steel reinforcement subjected to low-velocity impact loading.* Composite Structures, 2015. 126: 233-245.

[10]. Al-Rifaie, A., Guan, Z.W., Jones, S.W., and Wang, Q., *Lateral impact response of end-plate beam-column connections.* Engineering Structures, 2017. 151: 221-234.

[11]. Al-Rifaie, A., Jones, S.W., Wang, Q.Y., and Guan, Z.W., *Experimental and numerical study on lateral impact response of concrete filled steel tube columns with end plate*

connections. International Journal of Impact Engineering, 2018. 121: 20-34.

[12]. Saatci, S. and Vecchio, F.J., *Effects of shear mechanisms on impact behavior of reinforced concrete beams.* ACI structural Journal, 2009. 106(1): 78-86.

[13]. Tachibana, S., Masuya, H., and Nakamura, S., *Performance based design of reinforced concrete beams under impact.* Natural Hazards and Earth System Sciences, 2010. 10(6): 1069-1078.

[14]. Yan, Q., Sun, B., Liu, X., and Wu, J., *The effect of assembling location on the performance of precast concrete beam under impact load.* Advances in Structural Engineering, 2018. 21(8): 1211-1222.

[15]. Isaac, P., Darby, A., Ibell, T., and Evernden, M., *Experimental investigation into the force propagation velocity due to hard impacts on reinforced concrete members.* International Journal of Impact Engineering, 2017. 100: 131-138.

[16]. Yoo, D.-Y. and Banthia, N., *Size-dependent impact resistance of ultra-high-performance fiber-reinforced concrete beams.* Construction and Building Materials, 2017. 142: 363-375.

[17]. Dey, V., Bonakdar, A., and Mobasher, B., *Low-velocity flexural impact response of fiber-reinforced aerated concrete.* Cement and Concrete Composites, 2014. 49: 100-110.

[18]. Wang, W., Wu, C., Li, J., Liu, Z., and Lv, Y., *Behavior of ultra-high performance fiber-reinforced concrete (UHPFRC) filled steel tubular members under lateral impact loading.* International Journal of Impact Engineering, 2019. 132: 103314.

[19]. Ulzurrun, G.S.D. and Zanuy, C., *Enhancement of impact performance of reinforced concrete beams without stirrups by adding steel fibers.* Construction and Building Materials, 2017. 145: 166-182.

[20]. Zhou, X., Zhang, R., Xiong, R., Zhang, G., and Wang, X., *An Experimental Study of the Impact Mechanical Properties of RC Beams following Replacements of Stainless Steel Reinforcements of Equal Strength.* Advances in Materials Science and Engineering, 2019. 2019.

[21]. Lee, J.-Y., Shin, H.-O., Yoo, D.-Y., and Yoon, Y.-S., *Structural response of steel-fiber-reinforced concrete beams under various loading rates.* Engineering Structures, 2018. 156: 271-283.

[22]. Pham, T.M. and Hao, H., *Impact Behavior of FRP-Strengthened RC Beams without Stirrups.* Journal of Composites for Construction, 2016. 20(4): 04016011.

[23]. Wu, M., Zhang, C., and Chen, Z., *Drop-weight tests of concrete beams prestressed with unbonded tendons and meso-scale simulation.* International Journal of Impact Engineering, 2016. 93: 166-183.

[24]. Yilmaz, M., Anil, Ö., Alyavuz, B., and Kantar, E., *Load displacement behavior of concrete beam under monotonic static and low velocity impact load.* International Journal of Civil Engineering, 2014. 12(4): 488-503.

[25]. Jin, L., Zhang, R., Dou, G., Xu, J., and Du, X., *Experimental and numerical study of reinforced concrete beams with steel fibers subjected to impact loading.* International Journal of Damage Mechanics, 2018. 27(7): 1058-1083.

[26]. Bhatti, A.Q., Kishi, N., Konno, H., and Mikami, H., *Elasto-plastic dynamic response analysis of prototype RC girder under falling-weight impact loading considering mesh size*

effect. Structure and Infrastructure Engineering, 2012. 8(9): 817-827.

[27]. Liu, B., Fan, W., Guo, W., Chen, B., and Liu, R., *Experimental investigation and improved FE modeling of axially-loaded circular RC columns under lateral impact loading.* Engineering Structures, 2017. 152: 619-642.

[28]. Wang, R., Han, L.-H., and Hou, C.-C., *Behavior of concrete filled steel tubular (CFST) members under lateral impact: Experiment and FEA model.* Journal of Constructional Steel Research, 2013. 80(Supplement C): 188-201.

[29]. Deng, Y., Tuan, C.Y., and Xiao, Y., *Flexural Behavior of Concrete-Filled Circular Steel Tubes under High-Strain Rate Impact Loading.* Journal of Structural Engineering, 2012. 138(3): 449-456.

[30]. Xu, B. and Zeng, X., *Experimental study on the behaviors of reinforced concrete beams under impact loadings.* China Civil Engineering Journal, 2014. 47(2): 41-51.

[31]. Guo, J., et al., *Dynamic behaviour and energy dissipation of reinforced recycled aggregate concrete beams under impact.* Construction and Building Materials, 2019. 214: 143-157.

[32]. Guo, J., Cai, J., and Chen, W., *Inertial effect on rc beam subjected to impact loads.* International Journal of Structural Stability and Dynamics, 2017. 17(04): 1750053.

[33]. Li, H., Chen, W., and Hao, H., *Dynamic response of precast concrete beam with wet connection subjected to impact loads.* Engineering Structures, 2019. 191: 247-263.

[34]. Jin, L., Xu, J., Zhang, R., and Du, X., *Numerical study on the impact performances of reinforced concrete beams: A mesoscopic simulation method.* Engineering Failure Analysis, 2017. 80: 141-163.

[35]. Jiang, H., Wang, X., and He, S., *Numerical simulation of impact tests on reinforced concrete beams.* Materials & Design, 2012. 39: 111-120.

[36]. Wongmatar, P., Hansapinyo, C., Vimonsatit, V., and Chen, W., *Recommendations for Designing Reinforced Concrete Beams Against Low Velocity Impact Loads.* International Journal of Structural Stability and Dynamics, 2018: 1850104.

[37]. Zhang, C., Gholipour, G., and Mousavi, A.A., *Nonlinear dynamic behavior of simply-supported RC beams subjected to combined impact-blast loading.* Engineering Structures, 2019. 181: 124-142.

[38]. Li, J. and Hao, H., *Numerical study of concrete spall damage to blast loads.* International Journal of Impact Engineering, 2014. 68(Supplement C): 41-55.

[39]. Pham, T.M. and Hao, H., *Influence of global stiffness and equivalent model on prediction of impact response of RC beams.* International Journal of Impact Engineering, 2018. 113: 88-97.

[40]. Hao, Y. and Hao, H., *Influence of the concrete DIF model on the numerical predictions of RC wall responses to blast loadings.* Engineering Structures, 2014. 73: 24-38.

[41]. Chen, W., Hao, H., and Chen, S., *Numerical analysis of prestressed reinforced concrete beam subjected to blast loading.* Materials & Design, 2015. 65: 662-674.

[42]. Li, J., Hao, H., and Wu, C., *Numerical study of precast segmental column under blast loads.* Engineering Structures, 2017. 134: 125-137.

[43]. Do, T.V., Pham, T.M., and Hao, H., *Dynamic responses and failure modes of bridge columns under vehicle collision.* Engineering Structures, 2018. 156: 243-259.

[44]. Malvar, L.J., *Review of static and dynamic properties of steel reinforcing bars.* Materials Journal, 1998. 95(5): 609-616.
[45]. Hallquist, J.O., *LS-DYNA theory manual.* Livermore software Technology corporation, 2006: 531.
[46]. Rabczuk, T., Zi, G., Bordas, S., and Nguyen-Xuan, H., *A simple and robust three-dimensional cracking-particle method without enrichment.* Computer Methods in Applied Mechanics and Engineering, 2010. 199(37-40): 2437-2455.
[47]. Rabczuk, T., Bordas, S., and Zi, G., *On three-dimensional modelling of crack growth using partition of unity methods.* Computers & structures, 2010. 88(23-24): 1391-1411.
[48]. Zhao, D., Yi, W., and Kunnath, S.K., *Numerical simulation and shear resistance of reinforced concrete beams under impact.* Engineering Structures, 2018. 166: 387-401.
[49]. Adhikary, S.D., Li, B., and Fujikake, K., *Low Velocity Impact Response of Reinforced Concrete Beams: Experimental and Numerical Investigation.* International Journal of Protective Structures, 2015. 6(1): 81-111.
[50]. Pham, T.M. and Hao, H., *Effect of the plastic hinge and boundary conditions on the impact behavior of reinforced concrete beams.* International Journal of Impact Engineering, 2017. 102: 74-85.